IEEE Access
Multidisciplinary ⋮ Rapid Review ⋮ Open Access Journal

Received February 27, 2021, accepted March 12, 2021, date of publication March 19, 2021, date of current version April 6, 2021.

Digital Object Identifier 10.1109/ACCESS.2021.3067448

Development of Optimal Parameter Estimation Methodologies Applied to a 3DOF Autonomous Surface Vessel

ACCACIO FERREIRA DOS SANTOS NETO[1], LEONARDO DE MELLO HONÓRIO[2], MATHAUS FERREIRA DA SILVA[2], IVO CHAVES DA SILVA JUNIOR[2], AND LUIZ GUSTAVO FORTES WESTIN[3]

[1]Federal Center for Technological Education of Minas Gerais, Leopoldina 36700-000, Brazil
[2]Department of Electrical Energy, Federal University of Juiz de Fora, Juiz de Fora 36036-900, Brazil
[3]Itapebi Generation, Neoenergia Group, Rio de Janeiro 22210094, Brazil

Corresponding author: Leonardo de Mello Honório (leonardo.honorio@ufjf.edu.br)

This work was supported by the Interdisciplinary Research and Development Project undertaken by UFJF, and financed by UFJF, Coordenação de Aperfeicoamento de Pessoal de Nível Superior (CAPES), Conselho Nacional de Desenvolvimento Científico e Tecnológico (CNPq), and NEOENERGIA under supervision of ANEEL - The Brazilian Regulatory Agency of Electricity, under Project PD 00453-0017/2017.

ABSTRACT Autonomous Surface Vessels (ASVs) are reliable and robust vehicles. They perform autonomous missions in lakes, rivers and even open waters. Those are dangerous environments that requires precise and secure navigation. Under these conditions, the knowledge of a robust and accurate mathematical model is a fundamental aspect for adjusting the control system for reaching safety and performance. Moreover, traditional mathematical models disregard assimetries and coupling between the degrees of freedom. While those models work fine for bigger vessels, to ignore these characteristics in small ASVs compromises the model's quality. In this context, this work presents a new methodology for modeling and identifying the dynamics of ASVs along with the uncertainties arising from disturbances and non-modeled dynamics. As for the uncertainties and disturbances, this work considers the coupling parameters into the mathematical modeling, which synthesizes the divergences between the model and the real application, allowing to incorporate asymmetries and model deficiencies. Regarding the parameter identification, the proposal is based on (i) the design of optimal input excitation signals from a double layer optimization methodology and (ii) a parametric estimation concept in two steps, dividing the original set of parameters into two partially coupled sub-problems. Finally, this work also presents a full discussion and analysis about the importance to manage the trade-off between precision and complexity of mathematical models, its respective solution spaces and the impact over the optimization algorithms. To validate the approach, a real 3 Degree of Freedom ASV with aerial holonomic propulsion system is used. The results show that it is possible to successfully capture the complex set of parameters and identify physical characteristics not considered by the model.

INDEX TERMS Autonomous surface vehicles, real case parameter identification, 3 DOF ASV, optimal input signal design, solution space complexity management, parametric estimation.

I. INTRODUCTION

Marine surface vessels also known as Autonomous Surface Vessels ASVs, have attracted the attention of researchers around the world [1], [2].There are several advantages of using these ASV [1], [3]. They can perform dangerous missions, have reduced maintenance costs, greater potential capacity for payload, and high flexibility for monitoring and sampling in swallow or deeper waters.

Due to the potential mentioned above,this field of research has grown in the last two decades [1], [4], [5].Literature shows these vehicles operating in environments ranging from dams, rivers, lakes and open sea. They have been applied in: water and port supervision [6], shallow water hydrological survey [7], maritime search missions and rescue [8], among many other applications [1], [9].

The associate editor coordinating the review of this manuscript and approving it for publication was Juntao Fei.

However, ensuring that activities are performed reliably and safely is not a trivial task. In extreme situations, as in running water environments, the ASVs can be exposed to scenarios of great difficulties. Under these conditions, it is necessary a robust and reliable control strategy [10], [11].However, the designing of such controller is highly dependent on an accurate mathematical model, which enables to incorporate environmental disturbances and uncertainties.

The design of a proper nonlinear mathematical model presents tree main challenges [12]–[17]: ① ASV's traditional modeling disregard couplings and asymmetries, ② the high complexity of the solution space which lies the problem of optimal identification signal, and ③ the necessity of a robust numerical process to estimate the optimal parameters, ASV.

The advanced of embedded hardwares, precise sensors, robust propulsion systems, long range communications and other innovations has increased the development and application of several autonomous small ASVs [18], [19]. However, most of the mathematical modeling used to develop the low level control strategies are still based on large ships [20], [21]. Although this traditional modeling is a robust approximation, it disregards the coupling among the degrees of freedom and asymmetries that small robots are normally more sensitive. Moreover, these characteristics may be disregarded in large ships, however, they contribute to the final dynamics behavior in small vessels.

Regarding challenge ②, the optimal signal excites the vessel's main dynamics, so that these characteristics can be properly estimated [12], [16], [22]–[26]. The design of this signal requires intense persistence excitation such as the signals [12]: Pseudo-Random Binary Sequence (PRBS), Amplitude-Modulated Pseudo-Random Binary Signal (APRBS) and Filtered Gaussian Noise.

Despite this need for a signal with high persistence of excitation, it is observed that most studies related to ASVs, or even to marine vehicles in general, do not use this type of approach. Instead most works use low complexity signals as seen in [18], [19], [27].However different approaches are shown in [28]–[31] and [32], where the design of an optimal APRBS were presented. A major advanced shown in those approaches is the possibility of incorporating operational or safety constraints together with the optimization of the excitation persistence. It is a fact that, in principle, unplanned signals cannot guarantee.

In this context, this work presents the follow main contributions to the field of parametrical identification and field robotics involving ASVs;

- the introduction of coupling parameters generating a more precise and reliable mathematical model for small ASVs.
- An improved methodology for optimal exciting signal generation for parameter identification by integrating and adapting the concepts presented in [24], [25] and [28].
- A double step optimization approach that breaks the initial parameter set into two overlapped groups. This approach creates two reduced searching space, improving solvability.
- A real case application with a 3DOF ASVs vessel. In this real study, the mathematical model was identified and subsequently compared with experimental data.
- An in-deep walk-through from theoretical to practical analysis that provides valuable insights about the model identification process.

This paper is organized as follows: Section II presents the topology of the 3DOF ASV named AERO4River, showing all vehicle specifications and describing the traditional kinematics and dynamics modeling; Section III presents the parameter identification methodology; Section IV shows the application of the previous methodologies on the AERO4RIVER ASV; finally, Section V concludes this work.

II. ASV AERO4RIVER

A. TOPOLOGY

The developed vehicle has constructive characteristics that differ from a conventional catamaran. Its configuration uses a propulsion system with four aerial thrusters positioned at the top of the hull, with their axes of rotation parallel to the water surface, as illustrated in Fig. 1. This topology was first presented in [33], [34]. It provides an over-actuated ASV with eight actuators (four directional servos and four propulsion motors) and 3Degrees of Freedom (DoFs) (surge, sway and yaw).

FIGURE 1. Real view of the developed catamaran.

The aerial thrusters are more secure navigation options than conventional underwater ones. This feature enables the vessel to navigate in waters with solid waste without damage the propulsion system, and also does not influence the measurements of submerged sensors. Furthermore, the thrusters can be tilted from 0 to 360 degrees, ensuring 3 DoFs. A very important note at this point is, considering the number of DoFs along with its topology, the vessel responds very differently depending on the required forces and torques. This is a very difficult modeling problem where several dynamics are coupled together. In a mathematical point of view, this represents a high dimensional nonlinear solution space with several local minima. The search for the correct parameters

FIGURE 2. Motor rotation gear set.

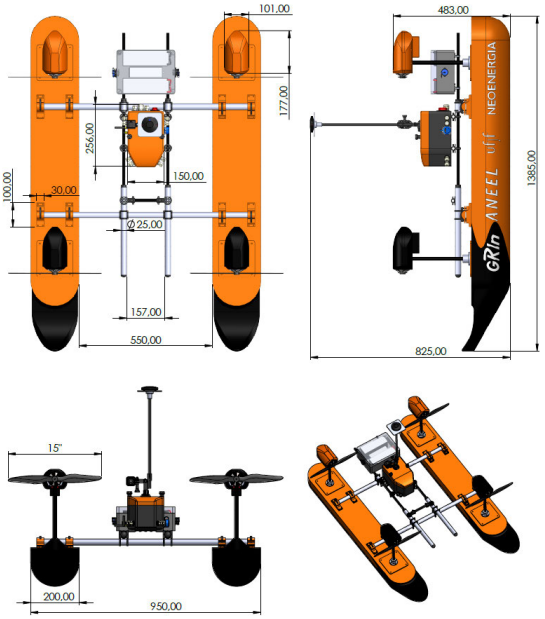

FIGURE 3. ASV technical drawing.

depends on how to represent this space, what parameters are considered and which is the best optimization strategy.

Figure 2 shows the configuration used to control the angular direction of each thruster, which is set by servomotors (in red) coupled to the support axes by gearboxes (yellow).

B. KINEMATICS AND DYNAMICS

The adopted model has 3 DoF, i.e., x and y axis translation movements (*Surge* and *Sway*) and rotation around the Z-Axis (*Yaw*). The remaining DoF are disregarded due to their small influence over the vessel's dynamics [1], [20].

The marine vehicle nomenclature is traditionally expressed as: $\boldsymbol{\eta} = [x, y, \psi]^T$ representing inertial (x, y) and angular (ψ) positions in the vehicle Inertial Frame $\mathcal{F}^I$; $\boldsymbol{\nu} = [u, v, r]^T$ being the linear (u, v) and angular (r) velocities in the Body-fixed Frame $\mathcal{F}^{BF}$ [20].

The general expressions that describe the vessel's dynamics and kinematic behaviors over the 3DoF movements are given by equations (1) and (2), respectively.

$$\boldsymbol{M}\dot{\boldsymbol{\nu}} + \boldsymbol{C}(\boldsymbol{\nu})\boldsymbol{\nu} + \boldsymbol{\tau_A} + \boldsymbol{\tau_D}\,\boldsymbol{C}\,\boldsymbol{g}(\boldsymbol{\eta}) = \boldsymbol{\tau} + \boldsymbol{\tau_E} \quad (1)$$

$$\dot{\boldsymbol{\eta}} = \boldsymbol{J}(\boldsymbol{\psi})\boldsymbol{\nu} \quad (2)$$

where $\boldsymbol{M} \in \mathbb{R}^{3\times3}$ is the Rigid Body Inertia Matrix, $\boldsymbol{C}(\boldsymbol{\nu}) \in \mathbb{R}^{3\times3}$ the Matrix of Coriolis, $\boldsymbol{J}(\cdot)$ the Jacobian matrix of velocities in the rigid body and inertial *frame*, and $\boldsymbol{\tau} \in \mathbb{R}^3$ represents the forces and moments generated by the propulsion system [33]. The contact between the water and the hull [20]generates added mass $\boldsymbol{\tau_A} \in \mathbb{R}^3$ and hydrodynamic damping $\boldsymbol{\tau_D} \in \mathbb{R}^3$. The restoration forces are represented by $\boldsymbol{g}(\boldsymbol{\eta}) \in \mathbb{R}^3$. $\boldsymbol{\tau_E} \in \mathbb{R}^3$ represents the environmental forces, colored noises and asymmetries whose vessel is exposed to (wind, waves and currents "oceanic or riverside"). Moreover,the matrices $\boldsymbol{J}$, $\boldsymbol{M}$ and $\boldsymbol{C}$ are represented by:

$$\boldsymbol{J}(\psi) = \begin{bmatrix} \cos(\psi) & -\sin(\psi) & 0 \\ \sin(\psi) & \cos(\psi) & 0 \\ 0 & 0 & 1 \end{bmatrix} \quad (3)$$

$$\boldsymbol{M} = \begin{bmatrix} m & 0 & 0 \\ 0 & m & mx_G \\ 0 & mx_G & I_z \end{bmatrix} \quad (4)$$

$$\boldsymbol{C}(\boldsymbol{\nu}) = \begin{bmatrix} 0 & 0 & -m(x_G r + v) \\ 0 & 0 & mu \\ m(x_G r + v) & -mu & 0 \end{bmatrix} \quad (5)$$

where m is the vehicle total mass, I_z is the z-axis moment of inertia, and x_G is the gravity center displacements on x axis.

1) HYDRODYNAMIC FORCES AND MOMENTS

The resulting hydrodynamic damping force is represented by the superposition of the linear, $\boldsymbol{D} \in \mathbb{R}^{3\times3}$, expressing contributions from potential damping and possible skin friction, and nonlinear $\boldsymbol{D_n}(\boldsymbol{\nu}) \in \mathbb{R}^{3\times3}$, associated with quadratic damping and higher order terms, expressed by the following equation [20]:

$$\boldsymbol{\tau_D} = \boldsymbol{D}\boldsymbol{\nu_r} + \boldsymbol{D_n}(\boldsymbol{\nu_r})\boldsymbol{\nu_r} \quad (6)$$

where $\boldsymbol{\nu_r} = \boldsymbol{\nu} - \boldsymbol{\nu_f}$, $\boldsymbol{\nu_r} \in \mathbb{R}^{3\times1}$ represents the relative velocity between the rigid and fluid, where $\boldsymbol{\nu_f} \in \mathbb{R}^{3\times1}$ represents the fluid velocity. $\boldsymbol{D}$ and $\boldsymbol{D_n}$ are expressed by:

$$\boldsymbol{D} = \begin{bmatrix} -X_u & -\overline{X}_v & -\overline{X}_r \\ -\overline{Y}_u & -Y_v & -\overline{Y}_r \\ -\overline{N}_u & -\overline{N}_v & -N_r \end{bmatrix} \quad (7)$$

$$\boldsymbol{D_n}(\boldsymbol{\nu}) = \begin{bmatrix} -X_{|u|u}|u| & -\overline{X}_{|u|v}|u| & -\overline{X}_{|u|r}|u| \\ -\overline{Y}_{|v|u}|v| & -Y_{|v|v}|v| & -\overline{Y}_{|v|r}|v| \\ -\overline{N}_{|r|u}|r| & -\overline{N}_{|r|v}|r| & -N_{|r|r}|r| \end{bmatrix} \quad (8)$$

considering the linear damping, X_u, Y_v, N_r represent the uncoupling linear parameters and the vessel's symmetry. Moreover, $\overline{X}_v, \overline{X}_r, \overline{Y}_u, \overline{Y}_r, \overline{N}_u, \overline{N}_v$ represent its asymmetries and express the linear relationship of damping for agiven movement direction. For large scale boats, these asymmetries are disregarded from the formulation. The terms D_n, $X_{|u|u}$, $Y_{|v|v}$, $N_{|r|r}$ represent the nonlinear symmetrical and uncoupling damping of a quadratic order in the directions of the x, y and z axes, respectively and all the others represent the asymmetries and couplings.

The added mass is treated by separating terms dependent on the accelerations and speeds of the body. Mathematically, the expression that is widely used in the literature is the following [21]:

$$\boldsymbol{\tau_A} = \boldsymbol{M_A}\dot{\boldsymbol{\nu}}_{\boldsymbol{r}} + \boldsymbol{C_A}(\boldsymbol{\nu_r})\boldsymbol{\nu_r} \quad (9)$$

where $\boldsymbol{\tau_A} \in \mathbb{R}^{3\times1}$ is the vector of forces and generalized moments of added mass, $\boldsymbol{M_A} \in \mathbb{R}^{3\times3}$ the Added Mass Matrix and $\boldsymbol{C_A(\nu)} \in \mathbb{R}^{3\times3}$ the Matrix of terms of Coriolis and Centripet added. The traditional representation of the matrices is given by [20]:

$$\boldsymbol{M_A} = \begin{bmatrix} X_{\dot{u}} & X_{\dot{v}} & X_{\dot{r}} \\ Y_{\dot{u}} & Y_{\dot{v}} & Y_{\dot{r}} \\ N_{\dot{u}} & N_{\dot{v}} & N_{\dot{r}} \end{bmatrix} \tag{10}$$

$$\boldsymbol{C_A(\nu)} = \begin{bmatrix} 0 & 0 & -\alpha_2 \\ 0 & 0 & \alpha_1 \\ \alpha_2 & -\alpha_1 & 0 \end{bmatrix} \tag{11}$$

$\boldsymbol{M}_A$ express the mass added in a given direction. Similarly to Equation (7) the diagonal parameters are related to uncoupling where the others represent coupling and asymmetries. Additionally, $\alpha_1 = X_{\dot{u}}.u + X_{\dot{v}}.v + X_{\dot{r}}.r$ and $\alpha_2 = Y_{\dot{u}}.u + Y_{\dot{v}}.v + Y_{\dot{r}}.r$.

for the sake of parameter set determination, it is possible to consider $\nu_f = 0$, so Equation (1) becomes

$$(\boldsymbol{M} + \boldsymbol{M_A})\dot{\boldsymbol{\nu}} + (\boldsymbol{C(\nu)} + \boldsymbol{C_A(\nu)} + \boldsymbol{D_n(\nu)})\boldsymbol{\nu} + \boldsymbol{D\nu} = \boldsymbol{\tau} + \boldsymbol{\tau_E} \tag{12}$$

As $\boldsymbol{M}, \boldsymbol{C(\nu)}$ and $\boldsymbol{C_A(\nu)}$ are related to already known variables, the parameter identification problem is resumed in finding $\boldsymbol{M_A}, \boldsymbol{D_n(\nu)}$ and $\boldsymbol{D}$. Moreover, non-modeled asymmetries will be considered as external forces or colored noise represented by $\boldsymbol{\tau_E}$. As this last one is not considered as parameter, the solution of the parameter identification lies on the $\mathbb{R}^{27}$ dimensional space.

III. IDENTIFICATION OF THE ASVs DYNAMICS

This section presents the general problem definition along with an analytical synthesis of possible approaches to improve solvability. Moreover, it is also presents the proposed method for modeling and identifying dynamic ASVs, which consists of two stages: (a) design of identification signals using the new approach called Robust SOESGOPE and, later, (b) parametric estimation in two phases. Note that, although the modeling and results consider the over-actuaded ASV presented in [33], [34], the proposed framework can be used for any other vessel.

A. PROBLEM DEFINITION

Consider a real vessel $\boldsymbol{\mathcal{R}(\Gamma)}$ which can be satisfactorily approximated by the nonlinear model $\boldsymbol{\mathcal{M}(\Gamma)}$, consisting of n states, p inputs, m outputs and r parameters, the response of this model for a given input signal $\boldsymbol{u}$ is represented by $\boldsymbol{\mathcal{M}(\Gamma, u)}$, and can is mathematically defined by:

$$\boldsymbol{\mathcal{M}(\Gamma, u)} := \begin{cases} \dot{\boldsymbol{x}}(t) = \boldsymbol{f}(\boldsymbol{x}(t), \boldsymbol{u}(t), \boldsymbol{\Gamma}) \\ \boldsymbol{y}(t) = \boldsymbol{h}(\boldsymbol{x}(t), \boldsymbol{u}(t), \boldsymbol{\Gamma}) \end{cases} \tag{13}$$

where $\boldsymbol{f}$ and $\boldsymbol{h}$ are the nonlinear functions that drives the system considering the state vector $\boldsymbol{x} \in \mathbb{R}^n$, the input vector $\boldsymbol{u} = [\tau_1, \tau_2, \cdots, \tau_k]$ where each $\tau_i \in \mathbb{R}^p$ is the acting forces over the system at moment t, the output vector $\boldsymbol{y} \in \mathbb{R}^m$ and the set of parameters of the model $\boldsymbol{\Gamma} \in \mathbb{R}^r$.

Also consider that the $\boldsymbol{\mathcal{R}(\Gamma, u)}$ system has some restrictions that need to be respected during its operation given the input signal $\boldsymbol{u}$, represented by:

$$\begin{aligned} \underline{\boldsymbol{x}} \leq \boldsymbol{x}(t) \leq \overline{\boldsymbol{x}} \\ \underline{\boldsymbol{y}} \leq \boldsymbol{y}(t) \leq \overline{\boldsymbol{y}} \\ \underline{\boldsymbol{u}} \leq \boldsymbol{u}(t) \leq \overline{\boldsymbol{u}} \end{aligned} \tag{14}$$

where $\underline{\boldsymbol{x}}$ and $\overline{\boldsymbol{x}} \in \mathbb{R}^n$ represent, respectively, the upper and lower operating limits of the vector states, $\underline{\boldsymbol{y}}$ and $\overline{\boldsymbol{y}} \in \mathbb{R}^m$ express the lower and upper operating limits of the vessel's output vector, respectively, while $\underline{\boldsymbol{u}}$ and $\overline{\boldsymbol{u}} \in \mathbb{R}^p$ represent the upper and lower operating limits of the input signal, respectively.

Also consider the function $\boldsymbol{\mathcal{P}}$ defined by

$$\boldsymbol{\mathcal{P}}(\boldsymbol{\mathcal{M}}(\hat{\boldsymbol{\Gamma}}^-, \boldsymbol{u}), [\boldsymbol{x}, \boldsymbol{y}]) = \hat{\boldsymbol{\Gamma}}^+ \tag{15}$$

as an arbitrary optimization procedure that uses the mathematical model $\boldsymbol{\mathcal{M}}$, the initial parameter estimation $\hat{\boldsymbol{\Gamma}}^-$, the state and output vectors $[\boldsymbol{x}, \boldsymbol{y}]$, and the signal $\boldsymbol{u} \in \boldsymbol{U}$ where $\boldsymbol{U}$ is the domain of all possible input signals, to estimate the parameter set $\hat{\boldsymbol{\Gamma}}^+$ which $\boldsymbol{\mathcal{M}}(\hat{\boldsymbol{\Gamma}}^+, \boldsymbol{u})$ best represents $[\boldsymbol{x}, \boldsymbol{y}]$. In this notation it is possible to replace $[\boldsymbol{x}, \boldsymbol{y}]$ by $\boldsymbol{\mathcal{M}(\Gamma, u)}$ or $\boldsymbol{\mathcal{R}(\Gamma, u)}$ without loss of generalization.

In this context, assume that $\boldsymbol{\Gamma}$ is the optimal, but unknown, set of system's parameters and that $\boldsymbol{\mathcal{M}(\Gamma)}$ best represents $\boldsymbol{\mathcal{R}(\Gamma)}$ for any given signal $\boldsymbol{u} \in \boldsymbol{U}$. Thus, the design of an optimal identification signal requires to find the best signal $\boldsymbol{u}^{\oplus} \in \boldsymbol{U}$ through an optimization search defined by

$$\boldsymbol{\mathcal{S}}(\boldsymbol{\mathcal{M}}(\hat{\boldsymbol{\Gamma}}^-), \boldsymbol{\mathcal{R}(\Gamma)}) = \boldsymbol{u}^{\oplus} \tag{16}$$

where $\boldsymbol{\mathcal{S}}$ is also an arbitrary mixed-integer optimization algorithm that searches for the best $\boldsymbol{u}^{\oplus} \in \boldsymbol{U}$. Finally, the optimal parameter set is defined by

$$\boldsymbol{\mathcal{P}}(\boldsymbol{\mathcal{M}}(\hat{\boldsymbol{\Gamma}}^-, \boldsymbol{u}^{\oplus}), \boldsymbol{\mathcal{R}}(\boldsymbol{\Gamma}, \boldsymbol{u}^{\oplus})) = \hat{\boldsymbol{\Gamma}}^+ \tag{17}$$

which generates the best *a posteriori* parameter estimation set $\hat{\boldsymbol{\Gamma}}^+$ where $\boldsymbol{\mathcal{M}}(\hat{\boldsymbol{\Gamma}}^+, \boldsymbol{u}) \approx \boldsymbol{\mathcal{R}(\Gamma, u)}$ for any other $\boldsymbol{u} \in \boldsymbol{U}$.

B. QUALITATIVE ANALYSIS FOR PARAMETER IDENTIFICATION

Before continue with the parameter identification methodology, it is important to expand the problem and its characteristics. As well known in literature and specifically shown in [25], [28] and [24] the parameter identification problem is highly sensitive to the excitation signal. As briefly shown in section III-A, the optimal designing of such signal is defined as a complex mixed-integer nonlinear optimization problem with an inner bounded nonlinear multimodal problem. While the outer looping demonstrated by Equation (16) is responsible for defining the optimal excitation signal $\boldsymbol{u}^{\oplus}$, the inner one defined by Equation (17) evaluates the optimal parameter set $\hat{\boldsymbol{\Gamma}}^+$. Moreover, each possible signal $\boldsymbol{u} \in \boldsymbol{U}$ generates a non-linear optimization problem with a different and unique

solution space. Thus, conceptually, the problem could be stated as to find the solution space that best excites the system and then, proceed with the parameter identification in a multimodal, but less complex non-linear space. Considering that the set $\boldsymbol{U}$ can be virtually infinite, this is a very complex and time consuming problem.

Considering the computational complexity, it was demonstrated for a toy problem in [25] that simpler mathematical models generates smaller solution spaces with could benefit the optimization process. It means that complex systems may be more representative, however, the system's complexity makes it computationally difficult to search for an optimal excitation signal.

Specifically for the ASV's parameters presented in 7, 8 and 10 the dimension of the inner solution space is $\mathbb{R}^{27}$ and the outer space size depends on the designed signal characteristics. Thus, considering $\boldsymbol{\Xi} \in \mathbb{R}^n$ a vector that encodes all necessary information to create an APRBS-like signal, the search space is defined by $3 \times \mathbb{R}^{27*n}$. The variable n must be sufficiently high to capture the system's dynamics and couplings, the scalar 27 represents this particular model, the scalar 3 represents the number of controllable DoF and, therefore, can be reduced in a way to capture the major characteristics without severely increasing the computational complexity.

Considering the above mentioned characteristics, this section presents a more robust approach for designing optimal input signals by using two different mathematical models; a simpler one for the signal design and a more complex one for the real parameter identification. Therefore, the first model will consider a symmetrical uncoupled system (only the diagonal terms) while the second one will also consider the asymmetries and couplings. This approach will reduce the solution space to $3 \times \mathbb{R}^{9*n}$.

C. EXCITATION SIGNALS DESIGNING

In many over-actuated dynamical systems, it is common to use the DoFs as controlled states instead of the real signals that are sent to the actuators [33]. This approach reduces the system's complexity and makes easier the control laws definition. Thus, the actions defined by the control system are forces and torques that act over the DoFs. In this work, the variable $\boldsymbol{\tau}$ represents the current (F_x, F_y, τ_ψ) forces acting over the surge and sway and torque over yaw, respectively. The real signals (f_1, f_2, f_3, f_4) representing the propulsion of each motor and $(\theta_1, \theta_2, \theta_3, \theta_4)$ the angle of each servo are evaluated by the fast control allocation procedure defined in [33]. It is very important to note that the allocation procedure could consider several different scenarios, including one where the servos are fixed and oriented towards surge only. In this particular scenario, although the ASV would have just two controllables Dof, the proposed identification frameworks would be almost the same; it would just have to consider $\boldsymbol{\tau} \in \mathbb{R}^2$. Figure 4 depicts this pipeline in an open looping scenario.

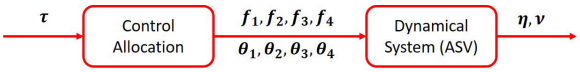

FIGURE 4. Control Allocation Scheme.

D. ORIGINAL SOESGOPE

The Sub-Optimal Excitation Signal Generation and Optimal Parameter Estimation (SOESGOPE) methodology was developed from the proof of the following hypothesis [28]: *"Assuming that a set* $\hat{\boldsymbol{\Gamma}}^-$ *is a rough, although valid, approximation of* $\boldsymbol{\Gamma}$*, then, if an optimal input signal* $\boldsymbol{u}^\oplus$ *can be used with* $\mathcal{M}(\hat{\boldsymbol{\Gamma}}^-)$ *to estimate* $\mathcal{M}(\tilde{\boldsymbol{\Gamma}}^p)$ *where* $\tilde{\boldsymbol{\Gamma}}^p$ *is a set of well known perturbed parameters used for benchmark, then* $\boldsymbol{u}^\oplus$ *is suitable for exciting* $\mathcal{R}(\boldsymbol{\Gamma})$ *such that a proper "a posteriori" estimation* $\hat{\boldsymbol{\Gamma}}^+$ *can be obtained."*

Moreover, reference [28] has also demonstrated that the search space of $\boldsymbol{u}^\oplus$ is only valid for an initial parameter set inside a trust region around $\hat{\boldsymbol{\Gamma}}^-$. These concepts can be better seen in Fig. 5, which presents the trust region surrounding the initial estimation $\hat{\boldsymbol{\Gamma}}^-$. The original SEOESGOPE proposes a two step approach. First to generate a well know perturbed parameter set $\tilde{\boldsymbol{\Gamma}}^p$ and use it as parameter to find $\boldsymbol{u}^\oplus$ and then, to use this excitation system on the real system $\mathcal{R}$ to find $\hat{\boldsymbol{\Gamma}}^+$.

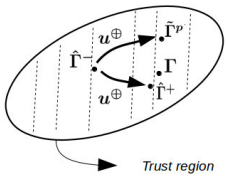

FIGURE 5. SOESGOPE concept.

Mathematically these steps can be defined as

$$\boldsymbol{u}^\oplus = \mathcal{S}(\mathcal{M}(\hat{\boldsymbol{\Gamma}}^-), \mathcal{M}(\tilde{\boldsymbol{\Gamma}}^p)) \tag{18}$$

$$\hat{\boldsymbol{\Gamma}}^+ = \mathcal{P}(\mathcal{M}(\hat{\boldsymbol{\Gamma}}^-, \boldsymbol{u}^\oplus), \mathcal{R}(\boldsymbol{\Gamma}, \boldsymbol{u}^\oplus)) \tag{19}$$

To design $\boldsymbol{u}^\oplus$, reference [28] has developed an optimization methodology using two well known optimization algorithms: the Meta-heuristic of Particle Swarm Optimization (PSO) [35] and the Interior Points Algorithm [36]. In this approach, the algorithms are arranged in a double layer strategy, with an external optimization layer specific to the signal design and an internal layer, dedicated to parameter estimation.

The outer layer is responsible for PSO and, therefore, dedicated to the optimization of APRBS signals. Each individual $\boldsymbol{\Xi}$ of the swarm is a signal candidate with different amplitudes and time intervals. Therefore, an APRBS signal designed of six stages, each one with pairs of (Amplitude, time interval). This designing strategy generates a the parameter's vector $\boldsymbol{\Xi} \in \mathbb{R}^{12}$, as shown in Fig. 6 where $\boldsymbol{\Xi} = [A_1, \ldots, A_6, t_1, \ldots, t_6]$ and $\boldsymbol{u}(\boldsymbol{\Xi})$ is the realization of these parameters, i.e. the signal marked as magenta.

The objective function used to find the optimal signal proposes the sum of specific metrics with different purposes. For the persistence of excitation, two metrics were used:

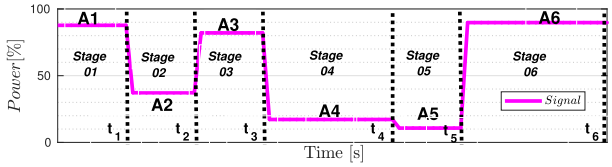

FIGURE 6. Parameterization of an APRBS signal.

- Precision Output Metric $f_o(\hat{\Gamma}^+)$: find the best set of parameter $\hat{\Gamma}^+$ that, for a given $\boldsymbol{u}(\Xi)$, minimizes the difference between the outputs and states obtained from $\mathcal{M}(\hat{\Gamma}^+, \boldsymbol{u}(\Xi))$ e $\mathcal{M}(\tilde{\Gamma}^p, \boldsymbol{u}(\Xi))$. This metric represents the inner layer shown in equation (17) and is mathematically described as:

$$\varepsilon := \sum_{k=0}^{t_u} ||\hat{\boldsymbol{x}}^+(k) - \tilde{\boldsymbol{x}}^p(k)|| + ||\hat{\boldsymbol{y}}^+(k) - \tilde{\boldsymbol{y}}^p(k)|| \quad (20)$$

  where $(\hat{\boldsymbol{x}}^+, \hat{\boldsymbol{y}}^+)$ and $(\tilde{\boldsymbol{x}}^p, \tilde{\boldsymbol{y}}^p)$ are the state and output of $\mathcal{M}(\hat{\Gamma}^+)$ e $\mathcal{M}(\tilde{\Gamma}^p)$, respectively, and t_u the duration of the signal.
- The Recoverability Metric $f_{\hat{\delta}}(\cdot)$ measures the capability to estimate the correct parameter set given $\boldsymbol{u}$ and $\tilde{\Gamma}^-$. Mathematically, $f_{\hat{\delta}}(\cdot)$ is represented by the sum of the relative error between the final estimation $\hat{\Gamma}^+$ and the reference $\tilde{\Gamma}^p$:

$$f_{\hat{\delta}}(\hat{\Gamma}^+, \tilde{\Gamma}^p | f_o) = \sum_{i=1}^{r} \frac{|\hat{\Gamma}_i^+ - \tilde{\Gamma}_i^p|}{|\tilde{\Gamma}_i^p|} \quad (21)$$

  where $\hat{\Gamma}_i^+$ e $\tilde{\Gamma}_i^p$ represent the i-th parameter of $\hat{\Gamma}^+$ and $\tilde{\Gamma}^p$. This metrics evaluate the similarity given de result provided by the former f_o metric. It is important once it is possible that completely different sets of parameters generate the same output. Thus, this metric observes how closely is the estimated parameters from the benchmark set.

The $\Theta(\cdot)$ penalizes a given signal $\boldsymbol{u}(\Xi)$ if it leads the system out of the desired operational constraints. Mathematically:

$$\Theta(\tilde{\boldsymbol{x}}^p, \tilde{\boldsymbol{y}}^p, t_u | \Xi) := \begin{cases} \dfrac{t_u}{K_1} + \dfrac{K_t f_V(\tilde{x}^p)}{K_1} + \dfrac{K_t f_V(\tilde{y}^p)}{K_1}, & \text{if } \sum \Psi(\cdot) \leq \alpha \\ \Psi(\tilde{x}^p) + \Psi(\tilde{y}^p) + \Psi(t_u) + 1, & \text{otherwise} \end{cases} \quad (22)$$

where a space function f_V used in experiment and$K_1 \gg K_t$, $\Psi(\cdot)$ is the penalty function and $\alpha \in \mathcal{R}$ is a relaxation index. It starts with $\alpha = 100$ and, in each iteration, it is assumed that $\alpha = 0.6\alpha$ such that $\alpha \longrightarrow 0$ at the end of the optimization process. So, the function $\Theta(\cdot)$ is based on α-constrain [37]. The penalty function is given by the system limitations.

Finally, using the metrics, [28] proposed to minimize the following objective function, composed of the weighted sum of the three metrics presented:

$$f(\Xi) = \underset{\Xi}{\text{Min}} \left(k_1 f_o(\cdot) + k_2 f_{\hat{\delta}}(\cdot) + k_3 \Theta(\cdot)\right) \quad (23)$$

where k_1, k_2 and $k_3 \in \mathcal{R}_{\geq 0}$ are constant weightings related to metrics and established according to priority.

E. ROBUST SOESGOPE

The new approach for designing identification signals is a derivation of the methodology originally developed by [28]. As [24] shows, the method is robust only when the initial estimation is valid. However, when the initial point does not represent the real system,the SOESGOPE does not provide good results. Moreover, to improve [28] the work [24] has proposed a sequential estimation methodology that performs a given mission, analyze the data and adjust the initial guess and operational limits. As this process is iterative until no further missions are required, it may be not suitable for real complex case scenarios. Fig. 7 where, due to uncertainties, the initial start point $\hat{\Gamma}^-$, the benchmark and the final *a posteriori* parameter set are outside the trust region which size is related to the system's complexity and nonlinearities.

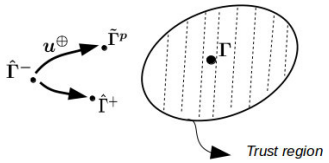

FIGURE 7. Initial guess outside of the trust region.

In this context, the modeling of an ASV has a high level of uncertainties in several hydrodynamic parameters, making to have an initial guess in a good region. Therefore, to increase performance and applicability, this work proposes a new derivation of SOESGOPE by adopting:

1) Use of multiple identification signals instead of one single signal. This approach increases the signal's excitation capacity, allowing to find the proper characteristics of the nonlinear dynamics system (NDS);
2) Establishment of restrictions only for the states of the NDS, concentrating the efforts into the signal's designing;

These modifications were designed to simplify the system by reducing its complexity, enhancing the capability of avoiding local minima and, therefore, making it more robust. By adopting multiple smaller signals means that each optimization problem will probably find a different local minimum and thus, will have more divisibility. This approach is a trade-off between precision and solvability and can be better seen in Fig. 8

Mathematically, the first proposal can be defined by the follow hypothesis: "if a parametric estimate *a priori* $\hat{\Gamma}^-$ vector generates a set of well spatially distributed benchmark parameters $\boldsymbol{P}^{\oplus} = [\tilde{\Gamma}_1^p, \tilde{\Gamma}_2^p, \ldots, \tilde{\Gamma}_n^p]$ to be applied to $\mathcal{M}(\boldsymbol{P}^{\oplus})$ it generates a series of signals $\boldsymbol{U}^{\oplus} = [\boldsymbol{u}_1^{\oplus}, \boldsymbol{u}_2^{\oplus}, \ldots, \boldsymbol{u}_n^{\oplus}]$ that are more likely to correctly estimate $\mathcal{R}(\Gamma)$."

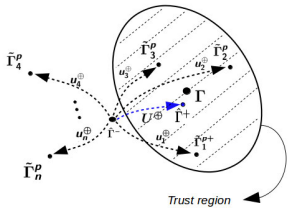

FIGURE 8. Multiple Signal Generation.

The second modification changes the evaluation metric $\Theta(\cdot)$ that now only establish constraints over the state variables;

$$\Theta(\tilde{\boldsymbol{x}}^p, \tilde{\boldsymbol{y}}^p | \boldsymbol{\Xi}) =: \begin{cases} \sum_{k=1}^{N} \sum_{i=1}^{n} \frac{|\tilde{x}_i^p(k) - \overline{x_i}|}{|\overline{x_i}|}, \forall \hat{x}_i^p(k) > \overline{x_i} \\ + \\ \sum_{k=1}^{N} \sum_{i=1}^{n} \frac{|\tilde{x}_i^p(k) - \underline{x_i}|}{|\underline{x_i}|}, \forall \hat{x}_i^p(k) < \underline{x_i} \\ + \\ \sum_{k=1}^{N} \sum_{i=1}^{m} \frac{|\tilde{y}_i^p(k) - \overline{y_i}|}{|\overline{y_i}|}, \forall \hat{y}_i^p < \overline{y_i} \\ + \\ \sum_{k=1}^{N} \sum_{i=1}^{m} \frac{|\tilde{y}_i^p(k) - \underline{y_i}|}{|\underline{y_i}|}, \forall \hat{y}_i^p < \underline{y_i} \end{cases} \tag{24}$$

F. REAL PARAMETRIC ESTIMATION

After the design and application of $\boldsymbol{U}^{\oplus}$ in $\mathcal{R}(\boldsymbol{\Gamma})$, the next step is the estimation of the vessel's parameters. As explained in subsections III-A and III-B, the ASV's identification problem can have up to 21 parameters, depending on the topology and hydrodynamic couplings.

The new estimation topology is different than the traditional ones found in the literature [12], [28]. Basically it defines an iterative and recursive two-phase parametric estimation solution with updates at the search limits parameters at each new iteration.

The two-phase approach creates two solution spaces reducing the individual complexity of each one improving the final convergence. This is a common tool in optimization [38], [39] that is now introduced by this work to the specific problem of parameter identification. Moreover, the limits are updated by a continuous iterative process. This is done by shifting the current range rather than just increasing it. Remembering that, as shown in [28], the limits expansion has a negative impact over the convergence process.

These concepts are detailed bellow.

1) Separate the original parameter set $\boldsymbol{\Gamma}$ into two subsets ($\hat{\boldsymbol{\Gamma}}_\alpha$ and $\hat{\boldsymbol{\Gamma}}_\beta$) whose swap solution brings healthy diversity to the optimization process;
2) Initialization of subsets: $\boldsymbol{\Gamma}_{\boldsymbol{\alpha}}^{-}$ and $\boldsymbol{\Gamma}_{\boldsymbol{\beta}}^{-}$;
3) 1^a Phase: "estimation of $\hat{\boldsymbol{\Gamma}}_\alpha$, considering $\boldsymbol{\Gamma}_\beta^+$ fixed variables";
4) 2^a Phase: "estimation of $\hat{\boldsymbol{\Gamma}}_\beta$, considering $\hat{\boldsymbol{\Gamma}}_\alpha^+$ fixed variables";
5) Adjust the search limits of the parameters according to the associated uncertainty. In this stage, the following treatment was adopted for both sets:

$$\overline{\hat{\boldsymbol{\Gamma}}} = \left(1 + \frac{\boldsymbol{\sigma}}{100}\right) \hat{\boldsymbol{\Gamma}}^+ \tag{25}$$

$$\underline{\hat{\boldsymbol{\Gamma}}} = \left(1 - \frac{\boldsymbol{\sigma}}{100}\right) \hat{\boldsymbol{\Gamma}}^+ \tag{26}$$

where $\boldsymbol{\sigma}$ represents the parametric uncertainty vector, $\underline{\hat{\boldsymbol{\Gamma}}}$ represents the lower limit and $\overline{\hat{\boldsymbol{\Gamma}}}$ the upper limit.
6) Return to the step ③ until the established number of iterations ends.

The final algorithm is shown below:

Algorithm 1 Two-Phase Parametric Estimation

Algorithm input information about $\mathcal{R}(\boldsymbol{\Gamma})$:
- Estimated *a priori* model: $\mathcal{M}(\hat{\boldsymbol{\Gamma}}^-)$;
- States and sign of the experiment: $\{\tilde{\boldsymbol{x}}^r, \tilde{\boldsymbol{y}}^r\}$ e $\boldsymbol{u}$;
- Definition and initialization of parameter sets: $\hat{\boldsymbol{\Gamma}}_\alpha^-$ e $\hat{\boldsymbol{\Gamma}}_\beta^-$

for $i = 1 : N$ **do** ▷ $N : n^o$ of estimation iterations
  Phase 01: $[\hat{\boldsymbol{\Gamma}}_\alpha^+] = f_{est}(\boldsymbol{x_0}, \hat{\boldsymbol{\Gamma}}_\alpha^-, \boldsymbol{x^r}, \boldsymbol{y^r}, \boldsymbol{u}, \hat{\boldsymbol{\Gamma}}_\beta^+)$
  Phase 02: $[\hat{\boldsymbol{\Gamma}}_\beta^+] = f_{est}(\boldsymbol{x_0}, \hat{\boldsymbol{\Gamma}}_\beta^-, \boldsymbol{x^r}, \boldsymbol{y^r}, \boldsymbol{u}, \hat{\boldsymbol{\Gamma}}_\alpha^+)$
  Parametric Update: $\hat{\boldsymbol{\Gamma}}_\alpha^- = \hat{\boldsymbol{\Gamma}}_\alpha^+$ e $\hat{\boldsymbol{\Gamma}}_\beta^- = \hat{\boldsymbol{\Gamma}}_\beta^+$
  Update of the limits of $\boldsymbol{\Gamma_\alpha}$ e $\boldsymbol{\Gamma_\beta}$
end for
Return: $\hat{\boldsymbol{\Gamma}}^+ = [\hat{\boldsymbol{\Gamma}}_\alpha^+, \hat{\boldsymbol{\Gamma}}_\beta^+]$

IV. RESULTS

In this section, it is presented the methods and applications of rSOESGOPE over the ASV AERO4River. All results are from real field missions and, due to the system's complexity, it is not possible to measure the performance by comparing the individual parameters as the way it was done in [28]. However, it is possible to analyze the real vessel's dynamics by comparing the linear and angular velocities with the ones provided by the mathematical models. For that, subsection IV-A shows the *a priori* model identification, which provides the initial set $\hat{\boldsymbol{\Gamma}}^-$, subsection IV-B shows the procedure to generate the set of optimal input signals $\boldsymbol{U}$, subsection IV-C shows the estimation procedure used to find $\hat{\boldsymbol{\Gamma}}^+$ along with comparisons with the orginal SOESGOPE, subsection IV-D compares the results of $\mathcal{M}(\hat{\boldsymbol{\Gamma}}^+)$ with the real ASV, i.e. $\mathcal{R}(\boldsymbol{\Gamma})$, for different input signals. The input signal uses all the eight available actuators on the ASV. For better compression, a practical step-by-step of the presented framework is described in Appendix A.

A. INITIAL PARAMETRIC ESTIMATION - AERO4RIVER

For this step it is necessary to have a simplified mathematical model $\mathcal{M}_s$ an initial estimate of the dynamic model

TABLE 1. Vessel operating characteristics.

DoF	Velocity			Propulsion	Unit
	Min	Max	Unit		
Surge	0.00	3.05	[m/s]	±78.00	[N]
Sway	-1.30	1.30	[rad/s]	±78.00	[N.m]
Yaw	-2.32	2.32	[rad/s]	±42.00	[N.m]

TABLE 2. Inertial parameters of the vessel.

Parameter	Value	Unit
m	$20,8000$	$[kg]$
I_z	$02,9824$	$[kg.m^2]$
x_g	$-0,0544$	$[m]$
y_g	$0,0000$	$[m]$

TABLE 3. Summary of the Priori Estimation $\mathcal{M}_s(\hat{\mathbf{\Gamma}}^-)$.

Parameter	$\mathcal{M}_s(\hat{\mathbf{\Gamma}}^-)$	Unit
$X_{\dot{u}}$	-9.82	$[kg]$
X_u	-0.00	$[kg/s]$
$X_{\|u\|u}$	-8.47	$[kg/m]$
$Y_{\dot{v}}$	-19.90	$[kg]$
Y_v	-0.00	$[kg/s]$
$Y_{\|v\|v}$	-24.95	$[kg/m]$
$N_{\dot{r}}$	-9.07	$[kg \cdot m^2/rad]$
N_r	-0.00	$[kg \cdot m^2/(rad \cdot s)]$
$N_{\|r\|r}$	-5.96	$[kg \cdot m^2/rad^2]$

parameters set $\hat{\mathbf{\Gamma}}^-$. The operational and inertial parameters, which are easier to evaluate through direct measures or CFD simulations were obtained. The results are shown in Tables 1 and 2, respectively.

To obtain the initial information about the main hydrodynamic parameters for the simpler nine variables uncoupled model, a test was performed using an APRBS based signal [40]. The results are shown in Table 3.

B. ROBUST SIGNAL DESIGNING

The first study is the definition of the signal stages number, i.e. the dimension of Ξ. The highest $dim(\Xi)$ is, the highest is the solution space and more difficult is to find a good signal. However, lower dimensions mean short excitation signals, which could make it difficult to capture the correct dynamics. To search for the optimum dimension size, each candidate was tested by using initial parameter set $\hat{\mathbf{\Gamma}}^-$ shown in table 3 along with 100 different perturbed benchmark $\tilde{\mathbf{\Gamma}}^p$ simulated systems.

The $\tilde{\mathbf{\Gamma}}^p$ was generated from the uncertainty (50%) attributed to the parameters, defined by the following equation:

$$\tilde{\mathbf{\Gamma}}^p = \left(1 + \frac{\sigma}{100}\boldsymbol{r_1}\right)\hat{\mathbf{\Gamma}}^- \tag{27}$$

where $\boldsymbol{\sigma} \in \mathbb{R}$ represents the level of parametric uncertainty between $[0, 100]$ and $\boldsymbol{r_1} \in \mathbb{R}^{9\times 1}$ is a vector of random numbers with uniform distributions between $[-1, 1]$.

TABLE 4. RMSE Result.

-	$\boldsymbol{u_1^{\oplus}}$	$\boldsymbol{u_2^{\oplus}}$	$\boldsymbol{u_3^{\oplus}}$
Ξ_{03}	0.0136	0.0788	0.0085
Ξ_{06}	0.0051	0.0088	0.0014
Ξ_{12}	1.1776	0.2591	0.0094
Ξ_{24}	2.8480×10^5	0.7757×10^5	0.6860×10^5
Ξ_{48}	8.2999×10^7	1.3730×10^7	7.3193×10^7

TABLE 5. Operational constraints.

-	Inferior Limit	Upper Limit	Unit
ψ	-6π	6π	[rad]
u	0.0	3.0	[m/s]
v	-1.0	1.0	[m/s]
r	-2.0	2.0	[rad/s]

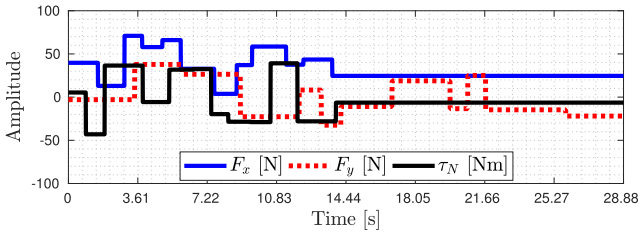

FIGURE 9. APRBS Signal $u_3^{\oplus}$.

The results of related to the Root-Mean Square Error (RMSE) for the best 3 signals of each run are shown in table 4. It is possible to conclude that the best number of stages is 6 and, for values over 24, the optimization problem diverges.

Thus, the settings used to identify the dynamics of the real AERO4River ASV by using the Robust SOESGOPE method are:

- number of signals: 3
- PSO algorithm: population with 15 particles each one encoding a Ξ_6 signal; 100 generations as a stopping criterion;
- Interior Point Algorithm:$f_o < 10^{-2}$ stop criterion;
- Weightings of the objective function: $k_2 = 1$, $k_3 = 20$ and $k_1 = 200$;
- 50 % uncertainty about $\hat{\mathbf{\Gamma}}^-$ for the emulation of the system $\mathcal{M}_s(\tilde{\mathbf{\Gamma}}^p)$;
- The operational constraints are shown in Table 5.

1) APRBS SIGNALS

Table 6 shows the initial perturbed parameter sets $\tilde{\mathbf{\Gamma}}_1^p$, $\tilde{\mathbf{\Gamma}}_2^p$ and $\tilde{\mathbf{\Gamma}}_3^p$, used along with Ξ_{06} signal configuration to evaluate $\boldsymbol{u_1^{\oplus}}$, $\boldsymbol{u_2^{\oplus}}$ and $\boldsymbol{u_3^{\oplus}}$. The excitation characteristics of each signal are shown in Figures 9, 10 and 11, respectively.

C. COMPLETE MODEL PARAMETRIC ESTIMATION

After generating $\boldsymbol{U^{\oplus}} = [\boldsymbol{u_1^{\oplus}}, \boldsymbol{u_2^{\oplus}}, \boldsymbol{u_3^{\oplus}}]$, the next step is its application in $\mathcal{R}(\boldsymbol{\Gamma}, \boldsymbol{U^{\oplus}})$ for the parametric estimation (PE) using the methodology described in the section III-F.

TABLE 6. Optimization Results - $P^{\oplus}$.

-	$u_1^{\oplus}$	$u_2^{\oplus}$	$u_3^{\oplus}$
$X_{\dot{u}}$	-8.91	-11.41	-8.69
X_u	0.00	0.00	0.00
$X_{\|u\|u}$	-12.84	-5.84	-11.41
$Y_{\dot{v}}$	-18.62	-21.78	-15.01
Y_v	0.00	0.00	0.00
$Y_{\|v\|v}$	-31.20	-37.25	-29.33
$N_{\dot{r}}$	-09.71	-15.14	-09.84
N_r	0.00	0.00	0.00
$N_{\|r\|r}$	-7.62	-5.71	-5.94
$Time(s)$	28.88	21.40	26.77
f_o	0.08	0.10	0.09
$f_{\hat{\delta}}$	0.05	0.60	0.11
Θ	0.00	0.00	0.00

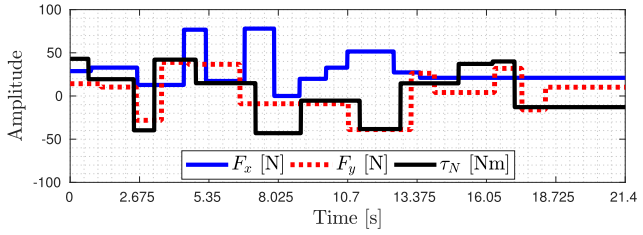

FIGURE 10. APRBS Signal $u_2^{\oplus}$.

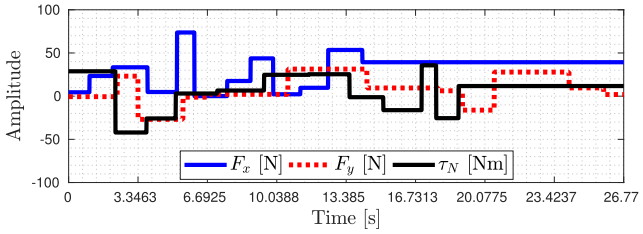

FIGURE 11. APRBS Signal $u_3^{\oplus}$.

The first task is to define the breaking sets. The 3 DoF with all possible couplings provides a model with 27 hydrodynamic parameters. For the sets definition, three scenarios were analyzed as described below and presented in the Table 7:

1) Model 0 (M0): original SOESGOPE;
2) Model 1 (M1): independent sets, $\mathbf{\Gamma_\alpha}$ groups the parameters of greatest contribution in the dynamics of ASV and $\mathbf{\Gamma_\beta}$ the others parameters related to couplings;
3) Model 2 (M2): dependent sets, whose common elements are the coupling parameters between the lateral and yaw movements and nonlinear damping, adding to $\mathbf{\Gamma_\alpha}$ the other parameters of direct influence on the dynamics of ASV and to $\mathbf{\Gamma_\beta}$ the remaining parameters;
4) Model 3 (M3): dependent sets, where the elements in common are the parameters of greatest contribution to the dynamics of the vessel, adding to $\mathbf{\Gamma_\alpha}$ and $\mathbf{\Gamma_\beta}$ the other parameters of drag and added mass, respectively;

Once defined the parameters sets ($\mathbf{\Gamma_\alpha}$, $\mathbf{\Gamma_\beta}$), the next step is to excite the real system $\mathcal{R}(\mathbf{\Gamma})$ with one given input

TABLE 7. Parameters set of study.

-	$\mathbf{\Gamma_\alpha}$	$\mathbf{\Gamma_\beta}$	$\mathbf{\Gamma_\alpha} \cap \mathbf{\Gamma_\beta}$
M1	$X_{\dot{u}}, X_u, X_{\|u\|u}$ $Y_{\dot{v}}, Y_v, Y_{\|v\|v}$ $N_{\dot{r}}, N_r, N_{\|r\|r}$	$X_{\dot{v}}, X_{\dot{r}}, X_v, X_r$ $Y_{\dot{u}}, Y_{\dot{r}}, Y_u, Y_r$ $N_{\dot{u}}, N_{\dot{v}}, N_u, N_v$ $X_{\|u\|v}, X_{\|u\|r}$ $Y_{\|v\|u}, Y_{\|v\|r}$ $N_{\|r\|u}, N_{\|r\|v}$	-
M2	$X_{\dot{u}}, X_u, X_{\|u\|u}$ $Y_{\dot{v}}, Y_v, Y_{\|v\|v}$ $N_{\dot{r}}, N_r, N_{\|r\|r}$	$X_{\dot{v}}, X_{\dot{r}}, X_v, X_r$ $Y_{\dot{u}}, Y_u$ $N_{\dot{u}}, N_u$	$Y_{\dot{r}}, Y_r, N_{\dot{v}}, N_v$ $X_{\|u\|v}, X_{\|u\|r}$ $Y_{\|v\|u}, Y_{\|v\|r}$ $N_{\|r\|u}, N_{\|r\|v}$
M3	X_v, X_v, Y_u Y_r, N_u, N_v $X_{\|u\|v}, X_{\|u\|r}$ $Y_{\|v\|u}, Y_{\|v\|r}$ $N_{\|r\|u}, N_{\|r\|v}$	$X_{\dot{v}}, X_{\dot{r}}$ $Y_{\dot{u}}, Y_{\dot{r}}$ $N_{\dot{u}}, N_{\dot{v}}$	$X_{\dot{u}}, X_u, X_{\|u\|u}$ $Y_{\dot{v}}, Y_v, Y_{\|v\|v}$ $N_{\dot{r}}, N_r, N_{\|r\|r}$

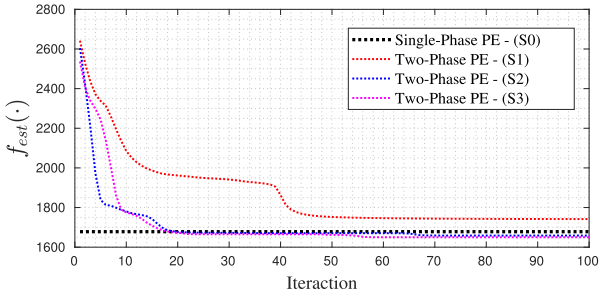

FIGURE 12. Study of parameter sets.

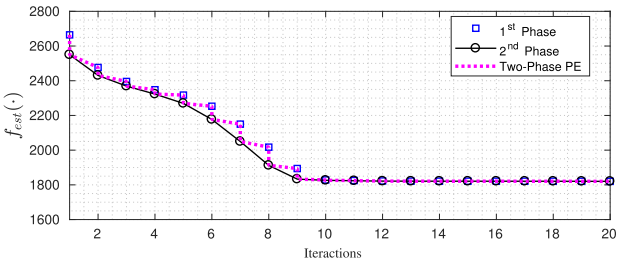

FIGURE 13. Evolution of f_{est}.

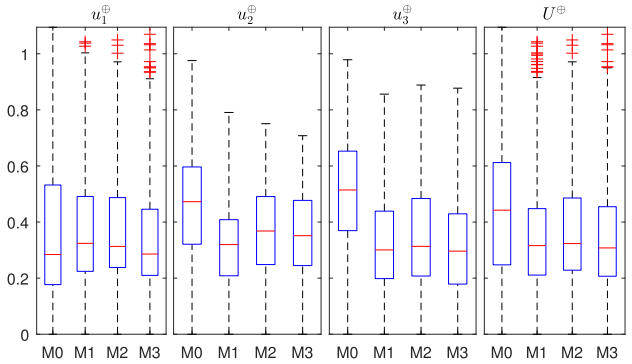

FIGURE 14. Linear Velocity RSE Results for Optimal Excitation Signal.

signal and to compare the convergence process of each set against the traditional Single-Phase PE. parameter estimation approach. Figure 12 shows these results for $\mathcal{R}(\mathbf{\Gamma}, \boldsymbol{U}^{\oplus})$, and it is possible to notice that the configurations M2 and M3 proved to be superior to the traditional method. Note that

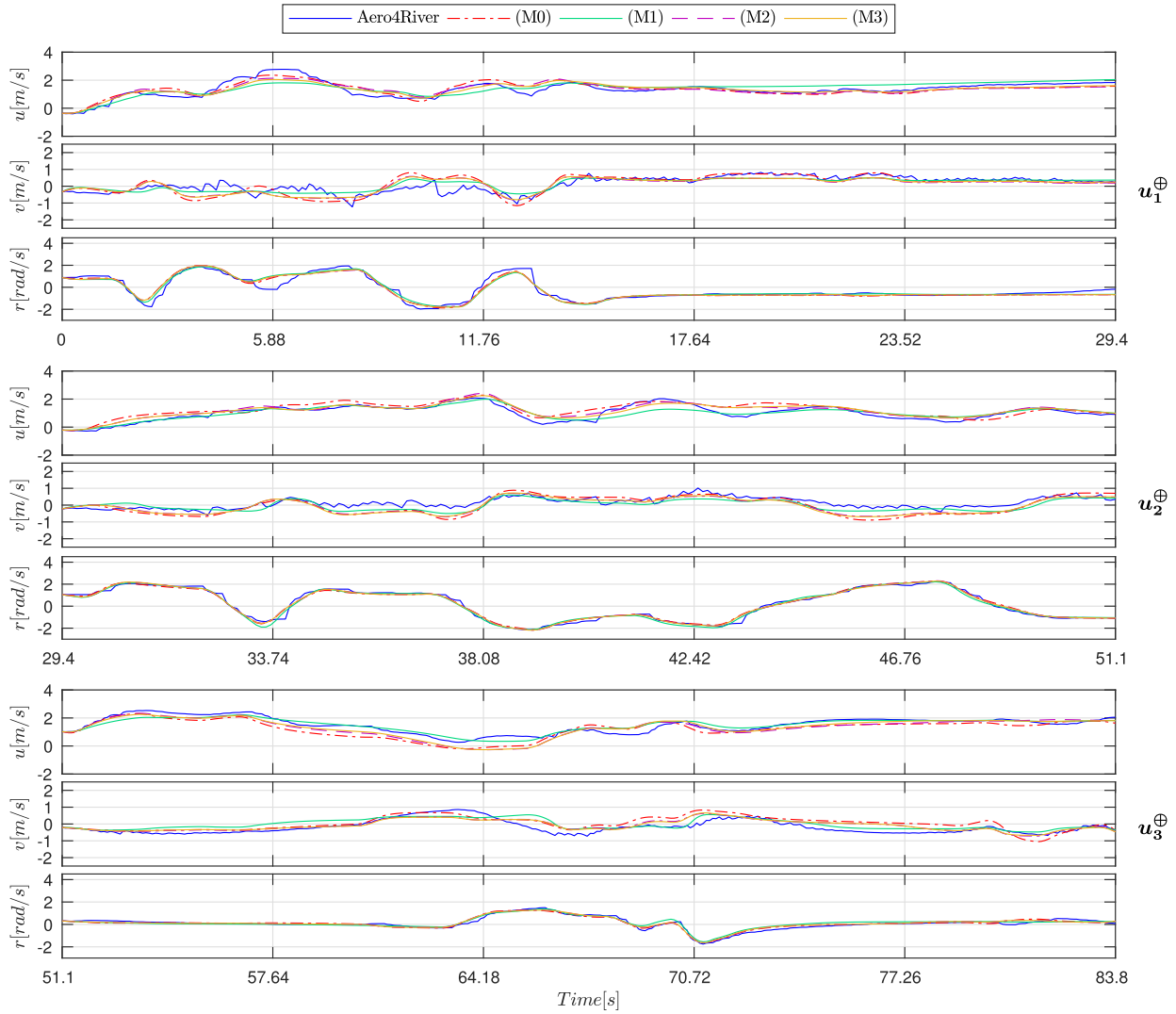

FIGURE 15. Estimated trajectory states using $U^{\oplus}$.

from 1^{st} iteration, the traditional method did not improve, suggesting the meeting of a local minimum. Different fact from study M3 (PE method in two phases) whose iterative process was beneficial up to approximately 60^{th} iteration, obtaining results superior to all studies.

The Two Phase PE technique convergence process is shown in Fig. 13. Note that the effect of the approach stimulates a slight disturbance in the optimization of f_{est}, providing beneficial effects to the process and mitigating premature convergence to minimum locations by emulation a predictor-corrector optimization algorithm. Moreover it is observed that as the iterative process continues, both phases converge to close values.

The final parameters sets identified by each approach using signal $\boldsymbol{U}^{\oplus}$ is shown in table 8

Figure 15 show a comparison between the velocities from each DoF (u, v, r - surge, sway and yaw) obtained from the modeling approaches (M_0, M_1, M_2, M_3) and the real ASV AERO4RIVER for signal $\boldsymbol{U}^{\oplus} = [\boldsymbol{u_1^{\oplus}}, \boldsymbol{u_2^{\oplus}}, \boldsymbol{u_3^{\oplus}}]$. In this figure, the signal $\boldsymbol{U}^{\oplus}$ was broken in three just to analyze the results for each individual part.

Analyzing the states in Fig 15 it is possible to see that the model obtained was able to identify the main dynamics of the 3 DoFs. Note that the DoF of *surge* and *yaw* obtained satisfactory results, while the DoF of *sway* diverged a little from the desired movement at times. This fact may have happened due to the low speed profile in the estimation, the presence of structural asymmetries and the lack of *roll* and *pitch* modeling not incorporated in the *priori* model.

It is also possible to see that the rSOESGOPE obtained better results, mainly in the DoFs relative to the frontal and lateral movements. In the yaw the original method was also efficient. In these movements, the new approach presents behaviors closer to the reality of the real vessel and very consistent in all experiments.

TABLE 8. Parametric Estimation Results from $\mathcal{R}(\Gamma, U^{\oplus})$.

-	$\hat{\Gamma}^{+}_{M0}$	$\hat{\Gamma}^{+}_{M1}$	$\hat{\Gamma}^{+}_{M2}$	$\hat{\Gamma}^{+}_{M3}$
$X_{\dot{u}}$	-4.79	-38.33	-12.84	-17.93
$\overline{X}_{\dot{v}}$	9.99	0.00	3.36	0.00
$\overline{X}_{\dot{r}}$	6.91	0.00	0.00	0.00
$\overline{Y}_{\dot{u}}$	-3.84	-34.67	-5.61	-6.67
$Y_{\dot{v}}$	-6.11	-33.35	-15.00	-19.93
$\overline{Y}_{\dot{r}}$	-6.29	0.00	-5.34	-5.37
$\overline{N}_{\dot{u}}$	-1.27	1.0614	0.00	0.00
$\overline{N}_{\dot{v}}$	-4.48	0.00	-5.60	-5.79
$N_{\dot{r}}$	-8.21	-7.62	-8.51	-8.49
X_u	-0.23	0.00	0.00	0.00
$\overline{X}_v$	-9.99	-70.46	-26.41	-39.93
$\overline{X}_r$	-10.00	0.00	-6.82	-4.77
$\overline{Y}_u$	1.44	0.00	0.00	0.00
Y_v	-9.99	0.00	0.00	0.00
$\overline{Y}_r$	-1.46	0.00	0.00	0.00
$\overline{N}_u$	-0.44	0.00	-0.94	-0.93
$\overline{N}_v$	-5.51	-10.86	-6.45	-6.89
N_r	-1.49	-2.49	-0.16	-0.00
$X_{\|u\|u}$	-8.89	-4.56	-8.76	-7.14
$\overline{X}_{\|u\|v}$	-2.22	49.22	0.00	16.06
$\overline{X}_{\|u\|r}$	4.18	-0.00	0.00	0.00
$Y_{\|v\|v}$	-43.66	-184.53	-170.17	-189.99
$\overline{Y}_{\|v\|u}$	-9.99	-0.00	-22.16	-22.47
$\overline{Y}_{\|v\|r}$	10.00	126.64	0.00	0.00
$N_{\|r\|r}$	9.99	0.00	3.36	-0.00
$\overline{Y}_{\|r\|u}$	-0.01	-1.01	0.00	0.00
$\overline{Y}_{\|r\|v}$	9.90	21.10	12.9570	13.30

TABLE 9. Linear Velocity RMSE Results for Optimal Excitation Signal (m/s).

-	$u_1^{\oplus}$	$u_2^{\oplus}$	$u_3^{\oplus}$	$U^{\oplus}$
M0	0.3702	0.3382	0.5463	0.4182
M1	0.3857	**0.2421**	**0.3565**	0.3281
M2	0.3753	0.2733	0.3881	0.3456
M3	**0.3529**	0.2668	0.3616	**0.3271**

Tables 9 and 10 show the final RMSE results considering the linear (m/s) and angular (rad/s) dynamics. These results were divided by the individual signals ($\boldsymbol{u_1^{\oplus}}, \boldsymbol{u_2^{\oplus}}, \boldsymbol{u_3^{\oplus}}$) with $\boldsymbol{U^{\oplus}}$ consolidating the final performance. Considering the linear dynamics, it is possible to notice that dealing with the couplings has improved the performance in each individual section. Moreover, the final rSOESGOEPE, considering M3, is 20% better than its original version. A small enhancement was also observed in the yaw dynamics, resulting in a better performance of 3%.

The complete Root Square Error (RSE) for the signals can be seen at Figs 14 and 16. The proposed modeling had lower dispersion around the RMSE result with the $M3$ approach been a little superior than its peers. The rSOESGOPE RMSE final result is aroud $0.3271 m/s$ and $0.1352 rad/s$ for the linear and angular dynamics. Considering the maximum linear velocity as $3 m/s$ this result represents an error about 11% of the real boat. Taking into account that it is a real open field experiment and so, subject to small but existing external forces, these are excellent results.

TABLE 10. Angular Velocity RMSE Results for Optimal Excitation Signal (rad/s).

-	$u_1^{\oplus}$	$u_2^{\oplus}$	$u_3^{\oplus}$	$U^{\oplus}$
M0	0.2054	0.0959	0.1207	0.1406
M1	**0.1977**	0.0987	0.1535	0.1499
M2	0.2124	0.0881	**0.1103**	0.1370
M3	0.2116	**0.0836**	**0.1103**	**0.1352**

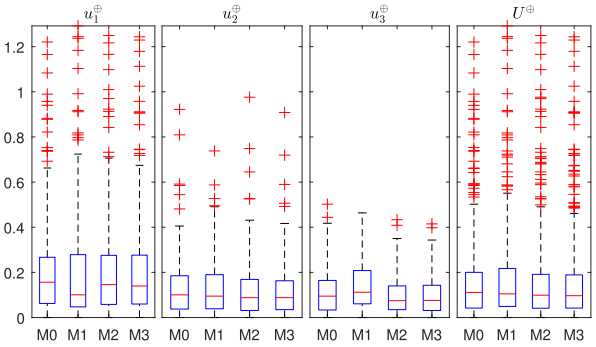

FIGURE 16. Angular Velocity RSE Results for Optimal Excitation Signal.

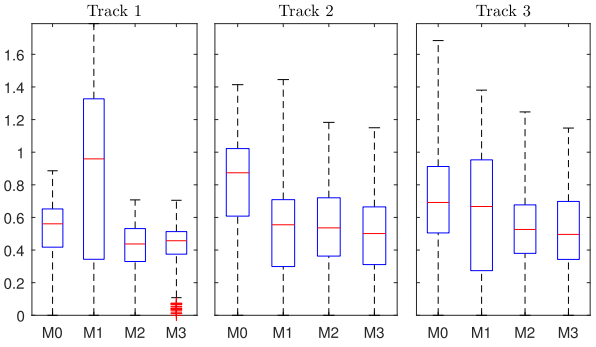

FIGURE 17. Linear Velocity RSE Results for Validation Tracks (m/s).

D. MODEL VALIDATION

Normally, works that deals with parametric identification that demonstrate the results in three ways; a) using the same training excitation signal for training and validation, b) different models for each individual signal or c) using well controlled experiments [2], [16], [18], [27], [32], [41], [42]. However, to demonstrate the practical performance of the proposed approach, two different sets were designed. The first, presented in section IV-C, represents in a machine learning taxonomy the training step. The second one, presented in this section, is the validation. Normally, training and validation signals are similar. However, for this domain, signals that are good for excite the system are likely not related to real missions. The other way is also a problem; real missions may not excite the system to capture its dynamics.

Thus, to validate the estimated models, this work will use maneuvering signals from three open looping field missions emulating real scenarios. Although the environment is a closed lake, noises such as minor water currents and wind are still present.

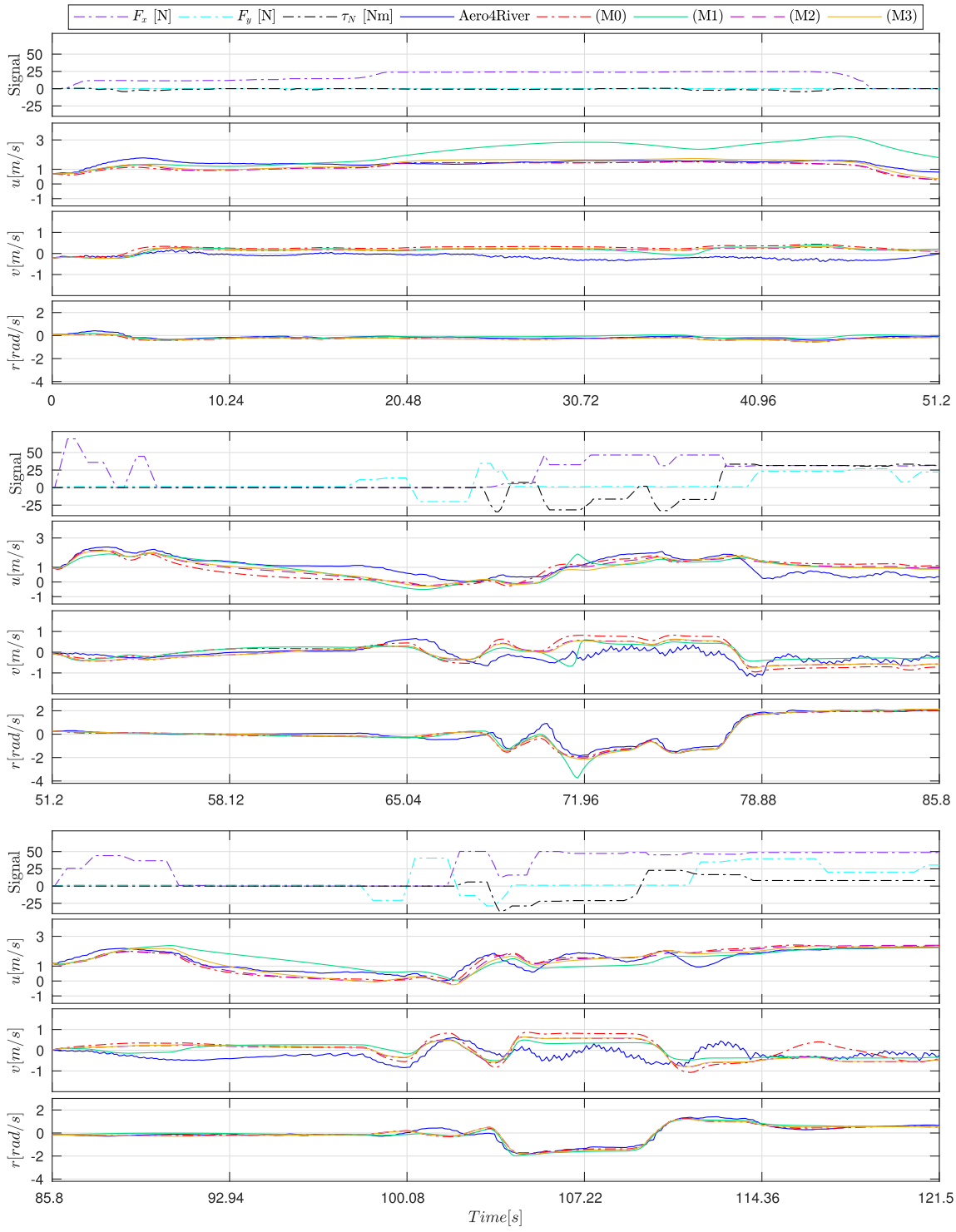

FIGURE 18. Excitation Signals and Estimated trajectory states for Tracks 1, 2 and 3.

1) DESIGNED TRACKS

The following tracks were heuristically designed to test the models. Tracks 1 and 2 represent real scenario inspections and track 3 emulates a feedback control output.

1) The first validation track consists of a strong frontal movement with minor yaw adjustments.
2) The second validation scenario analyzes the dynamics of the frontal and yaw movement together, simulating a zigzag movement.
3) The third and last scenario equally excites all dynamics in a pseudo-random movement emulating the output of a feedback control output for a given setpoints set.

TABLE 11. RMSE erros from the Estimated trajectory states - Linear Velocity (*m*/*s*).

-	Track 1	Track 2	Track 3
M0	0.5407	0.5488	0.5175
M1	0.8736	0.3769	0.4434
M2	**0.4253**	0.3657	0.3819
M3	0.4276	**0.3371**	**0.3671**

TABLE 12. RMSE erros from the Estimated trajectory states - Angular Velocity (*rad*/*s*).

-	Track 1	Track 2	Track 3
M0	0.1166	0.1485	**0.0989**
M1	**0.0954**	0.1471	0.1293
M2	0.1059	**0.1173**	0.1003
M3	0.1143	0.1192	0.1012

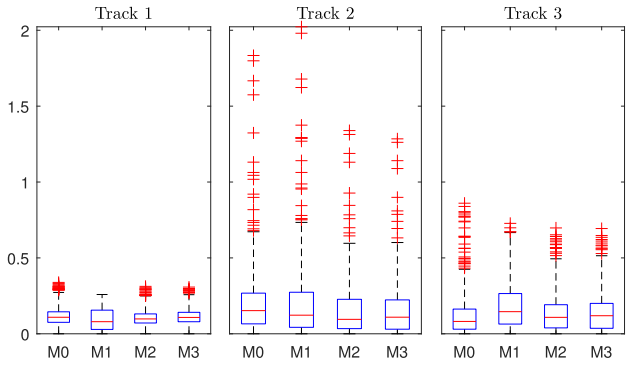

FIGURE 19. Angular Velocity RSE Results for Validation Tracks (*rad*/*s*).

Figure 18 shows the input signal $\boldsymbol{\tau} = [F_x, F_y, \tau_\psi]$ for each track; they directly feeds the control allocation module in a open looping strategy. The real model dynamics for the surge, sway and yaw velocities is represented by (u, v, r) respectively.

2) INTEGRATED ANALYSIS

Tables 11 and 12 show the RMSE results for the linear and angular velocities considering the four modeling strategies, and the three designed tracks. Models M2 and M3 have presented results almost up to 40% better than the original SOESGOPE (M0). The only scenario where the new modeling was inferior was in the M1 approach during track 1. In this case the surge dynamics was not properly captured. This is an important result once indicates that although the complete model is important, the optimization strategy used to solve the problem also makes the difference. Considering the angular velocities all models were able to capture well the dynamics in all tracks.

Figures 19 and 19 show the RSE result for the linear and angular velocities. Moreover, the error distribution in these two models were also more concentrated than models M0 and M1 for all tracks. The highest error of models M2 and M3 was lower than 1.45 m/s in the linear velocity. Disregarding the outliers, all models were able to capture the angular dynamics efficiently.

V. CONCLUSION

This work has presented a series of improvements for modeling and identification of small ASVs given the uncertainties and couplings arising from disturbances of the non-modeled dynamics.

Considering the ASV's dynamics, different from traditional approaches, all coupling variables were modeled and identified. Moreover, it was demonstrated that, for small ASV the couplings have a significant impact over the final model.

For the excitation signal, it was proposed and demonstrated that it is better, for the presented problem, to use a simplified mathematical modeling system. This approach reduces the solution space and is still able to capture the main dynamics of the ASV. Furthermore, it was also demonstrated that the signal size is important for optimal performance. While longer signals could provide richer excitation characteristics, the nonlinear solution space grows exponentially, making difficult for a traditional optimization algorithm to find a good instance.

Considering the final parameter estimation it was proposed to break the system in two overlaying sets to improve the convergence process. Although this approach is used in other domain problems such electrical power systems, it was introduced here for the problem of parametric estimation. Moreover, a new dynamic constraints range control was introduced and tested. The results of these two approces toghter have demonstrated that, by using two smaller but interconnected solution spaces and limiting its size through the desired ranges, the convergence process is slower, however with better results.

The final mathematical model was also tested in a real 3DoF ASV in a closed harbor environment operating different field missions. The results have shown a high similarity between the model developed by the proposed approach and the real system. This enhanced model can be now used to design robust control strategies and fault-tolerant systems to use the ASV in more hostile and demanding environments.

Finally the trade-off between precision and solvability was fully discussed and demonstrated during all this work and, although no fixed rule was proposed, it can be further exploring and testing several different ideas in future works. For instance, to study the performance of more robust multimodal optimization algorithms.

APPENDIX A

Algorithm 2 shows the practical high-level procedure to use the proposed framework. Although it was developed and tested for an ASV it can also be applied in asymptotically stable dynamical systems that can operate in an open looping strategy.

Algorithm 2 : General Step by Step Practical Procedure

1: Generate the simplified $\mathcal{M}_s$ and complete $\mathcal{M}$ mathematical models of the real dynamical system.
2: Obtain the initial parameter estimation $\hat{\mathbf{\Gamma}}^{-}$ for the simplified model through simulation softwares (openfoam®, solidworks®, etc.), real measures or analytical procedures.
3: Define practical operational constrains and a set of validation signals tracking $\boldsymbol{T}$ $\mathcal{D}$ $[\boldsymbol{tr_1}, \boldsymbol{tr_2}, \ldots, \boldsymbol{tr_n}]$.
4: Use the complete rSOESGOPE along with the simplified model to find $\boldsymbol{U}^{\oplus} = [\boldsymbol{u}_{\boldsymbol{1}}^{\oplus}, \boldsymbol{u}_{\boldsymbol{2}}^{\oplus}, \ldots, \boldsymbol{u}_{\boldsymbol{n}}^{\oplus}]$.
5: Apply $\boldsymbol{U}^{\oplus}$ and $\boldsymbol{T}$ in the real dynamical system $\mathcal{R}(\mathbf{\Gamma})$ by using an open looping approach, avoiding as much external disturbances as possible.
6: Use $\mathcal{R}(\mathbf{\Gamma}, \boldsymbol{U}^{\oplus})$, $\mathcal{M}$ and the rSOESGOPE estimation module to find $\hat{\mathbf{\Gamma}}^{+}$.
7: Use $\mathcal{M}(\hat{\mathbf{\Gamma}}^{+}, \boldsymbol{T})$ and $\mathcal{R}(\mathbf{\Gamma}, \boldsymbol{T})$ to validate the estimated parameters.

REFERENCES

[1] Z. Liu, Y. Zhang, X. Yu, and C. Yuan, "Unmanned surface vehicles: An overview of developments and challenges," *Annu. Rev. Control*, vol. 41, pp. 71–93, 2016.
[2] Z. Dong, X. Yang, M. Zheng, L. Song, and Y. Mao, "Parameter identification of unmanned marine vehicle manoeuvring model based on extended Kalman filter and support vector machine," *Int. J. Adv. Robotic Syst.*, vol. 16, no. 1, 2019, Art. no. 1729881418825095.
[3] S. Savitz, I. Blickstein, P. Buryk, R. W. Button, P. DeLuca, J. Dryden, J. Mastbaum, J. Osburg, P. Padilla, and A. Potter, "US Navy employment options for unmanned surface vehicles (USVs)," Rand Nat. Defense Res. Inst., Santa Monica, CA, USA, Tech. Rep. ADA588081, 2013.
[4] V. Bertram, "Unmanned surface vehicles-a survey," Skibsteknisk Selskab, Copenhagen, Denmark, Tech. Rep. 10.1.1.462.1894, 2008, pp. 1–14, vol. 1.
[5] J. E. Manley, "Unmanned surface vehicles, 15 years of development," in *Proc. OCEANS*, 2008, pp. 1–4.
[6] P. Mahacek, "Dynamic analysis of a SWATH vessel," MBARI, Moss Landing, CA, USA, Internship Rep., 2005, pp. 1–13.
[7] J. Curcio, J. Leonard, and A. Patrikalakis, "SCOUT–a low cost autonomous surface platform for research in cooperative autonomy," in *Proc. OCEANS MTS/IEEE*, Sep. 2005, pp. 725–729.
[8] H. Ferreira, R. Martins, E. Marques, J. Pinto, A. Martins, J. Almeida, J. Sousa, and E. P. Silva, "SWORDFISH: An autonomous surface vehicle for network centric operations," in *Proc. OCEANS-Eur.*, Jun. 2007, pp. 1–6.
[9] X. Sun, G. Wang, and Y. Fan, "Model identification and trajectory tracking control for vector propulsion unmanned surface vehicles," *Electronics*, vol. 9, no. 1, p. 22, Dec. 2019.
[10] S.-W. Ji, V. P. Bui, B. Balachandran, and Y.-B. Kim, "Robust control allocation design for marine vessel," *Ocean Eng.*, vol. 63, pp. 105–111, May 2013.
[11] M. F. Santos, L. M. Honorio, E. B. Costa, E. J. Oliveira, and J. P. P. G. Visconti, "Active fault-tolerant control applied to a hexacopter under propulsion system failures," in *Proc. 19th Int. Conf. Syst. Theory, Control Comput. (ICSTCC)*, Oct. 2015, pp. 447–453.
[12] R. Isermann and M. Münchhof, *Identification of Dynamic Systems: An Introduction With Applications*. New York, NY, USA: Springer, 2010.
[13] M. F. da Silva, L. M. Honório, A. L. M. Marcato, V. F. Vidal, and M. F. Santos, "Unmanned aerial vehicle for transmission line inspection using an extended Kalman filter with colored electromagnetic interference," *ISA Trans.*, vol. 100, pp. 322–333, May 2020.
[14] L. A. Aguirre, *Introdução à Identificação de Sistemas–Técnicas Lineares e Não-Lineares Aplicadas a Sistemas Reais*. Belo Horizonte, Brazil: Editora UFMG, 2004.
[15] D. D. A. Fernandes, A. J. Sørensen, K. Y. Pettersen, and D. C. Donha, "Output feedback motion control system for observation class ROVs based on a high-gain state observer: Theoretical and experimental results," *Control Eng. Pract.*, vol. 39, pp. 90–102, Jun. 2015.
[16] S. Wirtensohn, M. Schuster, and J. Reuter, "Disturbance estimation and wave filtering using an unscented Kalman filter," *IFAC-PapersOnLine*, vol. 49, no. 23, pp. 518–523, 2016.
[17] F. Deng, H.-L. Yang, and L.-J. Wang, "Adaptive unscented Kalman filter based estimation and filtering for dynamic positioning with model uncertainties," *Int. J. Control, Autom. Syst.*, vol. 17, no. 3, pp. 667–678, Mar. 2019.
[18] S. Wirtensohn, H. Wenzl, T. Tietz, and J. Reuter, "Parameter identification and validation analysis for a small USV," in *Proc. 20th Int. Conf. Methods Models Autom. Robot. (MMAR)*, Aug. 2015, pp. 701–706.
[19] M. Caccia, G. Bruzzone, and R. Bono, "A practical approach to modeling and identification of small autonomous surface craft," *IEEE J. Ocean. Eng.*, vol. 33, no. 2, pp. 133–145, Apr. 2008.
[20] T. I. Fossen, *Guidance and Control of Ocean Vehicles*, vol. 199. New York, NY, USA: Wiley, 1994.
[21] T. I. Fossen, *Handbook of Marine Craft Hydrodynamics and Motion Control*. Hoboken, NJ, USA: Wiley, 2011.
[22] L. Ljung, "Black-box models from input-output measurements," in *Proc. 18th IEEE Instrum. Meas. Technol. Conf. Rediscovering Meas. Age Inform. (IMTC)*, vol. 1, May 2001, pp. 138–146.
[23] T. I. Fossen and T. Perez, "Kalman filtering for positioning and heading control of ships and offshore rigs," *IEEE Control Syst.*, vol. 29, no. 6, pp. 32–46, Dec. 2009.
[24] M. B. Souza, L. D. M. Honório, E. J. D. Oliveira, and A. P. G. Moreira, "Recursive approach of sub-optimal excitation signal generation and optimal parameter estimation," *Int. J. Control, Automat. Syst.*, vol. 18, pp. 1965–1974, Feb. 2020.
[25] M. B. Souza, L. D. M. Honório, and E. J. Oliveira, "Innovative analysis for parameter estimation quality," *Int. J. Control, Automat. Syst.*, vol. 19, pp. 363–371, Sep. 2020.
[26] T. Weise, M. Zapf, R. Chiong, and A. J. Nebro, "Why is optimization difficult?" in *Nature-Inspired Algorithms for Optimisation*. New York, NY, USA: Springer, 2009, pp. 1–50.
[27] E. Revestido Herrero and F. J. Velasco González, "Two-step identification of non-linear manoeuvring models of marine vessels," *Ocean Eng.*, vol. 53, pp. 72–82, Oct. 2012.
[28] L. M. Honório, E. B. Costa, E. J. Oliveira, D. D. A. Fernandes, and A. P. G. M. Moreira, "Persistently-exciting signal generation for optimal parameter estimation of constrained nonlinear dynamical systems," *ISA Trans.*, vol. 77, pp. 231–241, Jun. 2018.
[29] C. Luo, S. I. McClean, G. Parr, L. Teacy, and R. De Nardi, "UAV position estimation and collision avoidance using the extended Kalman filter," *IEEE Trans. Veh. Technol.*, vol. 62, no. 6, pp. 2749–2762, Jul. 2013.
[30] E. J. Oliveira, L. M. Honório, A. H. Anzai, L. W. Oliveira, and E. B. Costa, "Optimal transient droop compensator and PID tuning for load frequency control in hydro power systems," *Int. J. Electr. Power Energy Syst.*, vol. 68, pp. 345–355, Jun. 2015.
[31] E. J. De Oliveira, C. A. Moraes, L. W. Oliveira, L. M. Honório, and R. P. B. Poubel, "Efficient hybrid algorithm for transmission expansion planning," *Electr. Eng.*, vol. 100, no. 4, pp. 2765–2777, Dec. 2018.
[32] N. M. Nouri, M. Valadi, and J. Asgharian, "Optimal input design for hydrodynamic derivatives estimation of nonlinear dynamic model of AUV," *Nonlinear Dyn.*, vol. 92, no. 2, pp. 139–151, Apr. 2018.
[33] M. F. da Silva, L. M. de Mello Honorio, M. F. dos Santos, A. F. dos Santos Neto, N. A. Cruz, A. C. C. Matos, and L. G. F. Westin, "Project and control allocation of a 3 DoF autonomous surface vessel with aerial azimuth propulsion system," *IEEE Access*, vol. 9, pp. 5212–5227, 2021.
[34] B. A. Regina, L. M. Honório, A. A. N. Pancoti, M. F. Silva, M. F. Santos, V. M. L. Lopes, A. F. S. Neto, and L. G. F. Westin, "Hull and aerial holonomic propulsion system design for optimal underwater sensor positioning in autonomous surface vessels," *Sensors*, vol. 21, no. 2, p. 571, Jan. 2021.
[35] R. Poli, J. Kennedy, and T. Blackwell, "Particle swarm optimization," *Swarm Intell.*, vol. 1, no. 1, pp. 33–57, Jun. 2007.
[36] R. H. Byrd, J. C. Gilbert, and J. Nocedal, "A trust region method based on interior point techniques for nonlinear programming," *Math. Program.*, vol. 89, no. 1, pp. 149–185, Nov. 2000.

[37] L. Honório, A. L. D. Silva, D. Barbosa, and L. Delboni, "Solving optimal power flow problems using a probabilistic α-constrained evolutionary approach," *IET Gener., Transmiss. Distrib.*, vol. 4, no. 6, pp. 674–682, 2010.
[38] E. J. Oliveira, L. W. Oliveira, J. L. R. Pereira, L. M. Honório, I. C. Silva, and A. L. M. Marcato, "An optimal power flow based on safety barrier interior point method," *Int. J. Electr. Power Energy Syst.*, vol. 64, pp. 977–985, Jan. 2015.
[39] C. Zhao, S. D. Round, and J. W. Kolar, "An isolated three-port bidirectional DC-DC converter with decoupled power flow management," *IEEE Trans. Power Electron.*, vol. 23, no. 5, pp. 2443–2453, Sep. 2008.
[40] M. Gringard and A. Kroll, "On the parametrization of APRBS and multisine test signals for the identification of nonlinear dynamic TS-models," in *Proc. IEEE Symp. Ser. Comput. Intell. (SSCI)*, Dec. 2016, pp. 1–8.
[41] S. Wirtensohn, J. Reuter, M. Blaich, M. Schuster, and O. Hamburger, "Modelling and identification of a twin hull-based autonomous surface craft," in *Proc. 18th Int. Conf. Methods Models Autom. Robot. (MMAR)*, Aug. 2013, pp. 121–126.
[42] J. Han, J. Xiong, Y. He, F. Gu, and D. Li, "Nonlinear modeling for a water-jet propulsion USV: An experimental study," *IEEE Trans. Ind. Electron.*, vol. 64, no. 4, pp. 3348–3358, Apr. 2017.

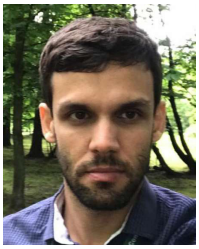

ACCACIO FERREIRA DOS SANTOS NETO received the M.Sc. degree in computational modeling from the Federal University of Juiz de Fora (UFJF), Brazil, in 2013, where he is currently pursuing the Ph.D. degree in electrical engineering. He is also a Professor with the Federal Center for Technological Education of Minas Gerais (CEFET-MG). His current research interests include engineering education, automatic control, system identification, and surface marine vehicles modeling.

LEONARDO DE MELLO HONÓRIO received the B.Sc. degree in electrical engineering from the Federal University of Juiz de Fora (UFJF), in 1993, and the M.Sc. and Ph.D. degrees in electrical engineering from EFEI, Brazil, in 1999 and 2002, respectively. He was a Visiting Researcher with the University of California at Irvine and Porto University, in 2006 and 2012, respectively. He is currently a Full Professor with UFJF. His current research interests include evolutionary algorithms, probabilistic methods, electrical power systems, robotics, autonomous vehicles, fuzzy logic, pattern recognition, and optimization.

MATHAUS FERREIRA DA SILVA received the B.Sc. degree in control and automation engineering from the Federal Center for Technological Education of Minas Gerais (CEFET-MG), in 2015, and the M.Sc. degree in electrical engineering from the Federal University of Juiz de Fora (UFJF), in 2017, where he is currently pursuing the Ph.D. degree with the Graduate Program in Electrical Engineering. He has been involved in research and development projects (R&D) in robotics with an emphasis on unmanned autonomous aerial vehicles (UAVs), and autonomous surface vehicles (ASVs) for more than a period of five years. His main research interests include unmanned aerial vehicles (UAVs), autonomous surface vehicles (ASVs), stochastic methods, navigation, control, automation, and optimization.

IVO CHAVES DA SILVA JUNIOR received the B.Sc. and M.Sc. degrees from the Federal University of Juiz de Fora (UFJF), Brazil, in 2001 and 2003, respectively, and the D.Sc. degree from COPPE, Federal University of Rio de Janeiro, Rio de Janeiro, Brazil, in 2008. Since 2009, he has been a Professor with the Electrical Engineering Department, UFJF. His research interests include power economics, optimization, and power systems analysis.

LUIZ GUSTAVO FORTES WESTIN is currently pursuing the master's degree in energy engineer from the Federal University of Itajuba - MG. He is also a Hydraulic Engineer Specialist in electric generation systems. He is working for the Neoenergia Group. He is also a specialist in dam safety by the Institute IDD, Curitiba. He has 14 years of experience in the electrical sector with activities focused on hydraulic and hydrology engineering, operation and civil-hydraulic maintenance in hydroelectric plants and dam safety with operations in the ENEL and Iberdrola Groups.